NON-LINEAR DEFORMED INTERFACE CORNER STRESS CHARACTERIZATION BY EFFECTIVE PARALLEL NUMERICAL METHODS

M. SCHERZER
Department of Mathematics, Technical University Chemnitz-Zwickau,
D-09107 Chemnitz, Germany

ABSTRACT

This paper provides stable and comparable solutions in general for two-dimensional geometrically linear statements of solid mechanics (isotropic elasticity, isotropic deformation theory, flow theory with isotropic hardening) at interface corners using eigenfunction expansions. The basic idea of the singular and non-singular stress and deformation field calculation is characterized by introducing stiffness actions which operate as the corner neighbourhood on the surrounding body and can be assembled in a common way to the global stiffness matrix of the body. An interesting fact is that these stiffness actions do not depend on the distance from the singularity point. All computations are made on modern parallel computers. Using Domain Decomposition as parallel computing concept an effective parallel preconditioned conjugate gradient method for high order degree of freedom finite element systems is utilized. In this connection the asymptotic stiffnesses mentioned above fit well for the applied parallel solution technique and lead to an improvement of the stiffness matrix condition. Concrete examples show the advantages of the presented approach. Deformation fracture criterions characterizing different local stress conditions at interface corner and crack configurations are introduced and discussed.

KEYWORDS

Interface corner (crack), non-linear deformation, effective parallel iterative solution technique, characterization of fracture stress states.

INTRODUCTION

Fracture applications for material compounds in micro-electronical and other structural members of high technologies require stable comparable solutions of correctly formulated boundary value problems in linear and non-linear solid mechanics on one side and corresponding experimental research for identification of material behaviour and determination of the critical parameters resulting from the solid models on the other.
It is very complicated to get these solutions in critical points of the solid because of the singular oscillation effects which may appear at interface corners and cracks. Introducing modified geometrical models of very small smooth circles instead of sharp corners to

get simple solid statements is not always succesful. It must be pointed out that singular solutions for solids with partly homogeneous material behaviour cannot be excluded in principle for all cases. For instance a circle smoothed interface crack has the singular behaviour of a 90°-90° material compound. On the other hand for very small circles it is necessary to include models of microscale levels which require extended experimental investigations and coupling theories to solid mechanics. In this connection the expense can only grow. As a first approximation the solid models with corresponding macroscopic experiments are responsible for fracture behaviour.

This paper provides the mentioned stable comparable solutions in general for two-dimensional geometrically linear statements of solid mechanics (isotropic elasticity, isotropic deformation theory, flow theory with isotropic hardening) at interface corners by eigenfunction expansions which are coupled to the usual finite element approach of the solid surrounding the corner. The applied technique allows extensions from incrementally proportional load paths to non-proportional local load increments simplifying the mathematical calculations for the presentation of stress and strain fields in this general case.

REPLACEMENT OF ASYMPTOTIC SOLUTION BY STIFFNESS ACTIONS

Let us consider two-dimensional statements in the neighbourhood of an interface corner consisting of two material ranges ($0 \le \theta \le \theta_o$ and $0 \ge \theta \ge -\theta_u$). At a distance of $\xi = \xi_0$ from the corner the finite element nodes of a regular net are established in a polar coordinate system of ξ and θ together with the displacement degrees of freedom $u_k(\xi_0, \theta_j)$ (see Fig. 1). For formulations of geometrically linear and physically non-linear isotropic

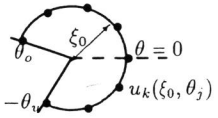

Fig. 1. Neighbourhood of an interface corner together with the finite element nodes

statements the following boundary conditions are given:

- Vanishing normal and tangent stresses $(\sigma_{\theta\theta}, \sigma_{\xi\theta})$ at $\theta = \theta_0, -\theta_u$
- Continuity of normal and tangent stresses and displacements (u_ξ, u_θ) at $\theta = 0$.

The main idea of the singular and non-singular stress and deformation field calculation at interface corners presented here characterizes a replacement of the corner neighbourhood ($\xi < \xi_0$) effect to the surrounding body ($\xi > \xi_0$) by introducing stiffness actions at $\xi = \xi_0$ which can be assembled in a conventional way together with the other element stiffness matrices to the global stiffness matrix of the body. For $\xi < \xi_0$ the following relations are valid:

$$\boldsymbol{\sigma} = \sum_i C_i \mathbf{f}_i^{(\sigma)}(\xi, \theta), \quad \boldsymbol{\sigma} = \{\sigma_{\xi\xi}, \quad \sigma_{\xi\theta}\}; \quad \boldsymbol{u} = \sum_i C_i \mathbf{f}_i^{(u)}(\xi, \theta), \quad \boldsymbol{u} = \{u_\xi, u_\theta\}. \tag{1}$$

In (1) $\mathbf{f}_i^{(\sigma)}(\xi, \theta) = \{f_{i\xi\xi}^{(\sigma)}(\xi, \theta), f_{i\xi\theta}^{(\sigma)}(\xi, \theta)\}$ and $\mathbf{f}_i^{(u)}(\xi, \theta) = \{f_{i\xi}^{(u)}(\xi, \theta), f_{i\theta}^{(u)}(\xi, \theta)\}$ denote the corresponding vectors of stress and displacement eigenfunctions whose concrete forms are given by Scherzer and Meyer (1996). In the case of flow theory applications in (1) the corresponding eigenfunctions for the increments of stresses and displacements have to be used in the way shown by Scherzer (1994) and Scherzer and Meyer (1996). Because of the boundary conditions at the circle $\xi = \xi_0$ it is not necessary to include the stress component

$\sigma_{\theta\theta}$ in $\boldsymbol{\sigma}$. The constants C_i can be related to $u_k(\xi_0, \theta_j)$ $(k = \xi, \theta)$ by

$$u_k(\xi_0, \theta_j) = \sum_i C_i f_{ik}^{(u)}(\xi_0, \theta_j), \quad (k = \xi, \theta; j = 1, 2, 3, ...) \tag{2}$$

and solving (2) one gets

$$C_i = \sum_j b_{ij}(\xi_0, \theta_1, ...) v_j(\xi_0), \qquad v_1(\xi_0) = u_\xi(\xi_0, \theta_1), v_2(\xi_0) = u_\theta(\xi_0, \theta_1),$$

$$v_3(\xi_0) = u_\xi(\xi_0, \theta_2), v_4(\xi_0) = u_\theta(\xi_0, \theta_2), v_5(\xi_0) = u_\xi(\xi_0, \theta_3), ...; \ \theta_1 = -\theta_u, ...\theta_N = \theta_o. \tag{3}$$

To obtain stiffness actions it is necessary to calculate the virtual work δA of stresses on the circle $\xi = \xi_0$:

$$\delta A = \xi_0 \int_{-\theta_u}^{\theta_o} \boldsymbol{\sigma} \bullet \delta \boldsymbol{u} \, d\theta = \xi_0 \sum_{i,j} \int_{-\theta_u}^{\theta_o} \mathbf{f}_i^{(\sigma)}(\xi_0, \theta) \bullet \mathbf{f}_j^{(u)}(\xi_0, \theta) \, d\theta C_i \delta C_j$$

$$\delta A = \sum_{k,l} \left[\xi_0 \sum_{i,j} b_{ik} b_{jl} \int_{-\theta_u}^{\theta_o} \mathbf{f}_i^{(\sigma)}(\xi_0, \theta) \bullet \mathbf{f}_j^{(u)}(\xi_0, \theta) \, d\theta \right] v_k(\xi_0) \delta v_l(\xi_0). \tag{4}$$

The symbol "•" marks scalar products of corresponding vectors. The kl (k-th column, l-th row) element of the wanted stiffness action matrix is determined in (4) as the factor of $v_k(\xi_0)\delta v_l(\xi_0)$ (bracket). Computations of stiffness actions by (2), (3) and (4) lead to an introduction of n eigenfunctions if n degrees of freedom exist at $\xi = \xi_0$. Avoiding this non-effective procedure it is possible to orthogonalize the eigenfunctions.

ORTHOGONALIZATION OF EIGENFUNCTIONS

Let us introduce a new system of functions $\mathbf{f}_i^{(\sigma)\sim}(\xi, \theta)$ and $\mathbf{f}_i^{(u)\sim}(\xi, \theta)$ from $\mathbf{f}_i^{(\sigma)}(\xi, \theta)$ and $\mathbf{f}_i^{(\sigma)}(\xi, \theta)$ which satisfies the conditions

$$\int_0^{\xi_0} \xi \left(\int_{-\theta_u}^{\theta_o} \mathbf{f}_i^{(\sigma)\sim}(\xi, \theta) \bullet \mathbf{f}_j^{(u)\sim}(\xi, \theta) \, d\theta \right) d\xi = \xi_0^2 \delta_{ij}, \quad (\delta_{ij} - \text{Kronecker's symbol}).$$

Using Schmidt's orthogonalization method which is for instance presented by G. Korn and T. Korn (1968) in connection with the condition above the representations of displacements, stresses and δA, according to Scherzer and Meyer (1996), follow in the form:

$$\boldsymbol{u}(\xi_0, \theta) = \sum_i \widetilde{C}_i(\xi_0) \sqrt{\xi_0} \mathbf{f}_{.i}^{(u)\sim}(\theta), \ \boldsymbol{\sigma}(\xi_0, \theta) = \sum_i \widetilde{C}_i(\xi_0) \frac{\mathbf{f}_{.i}^{(\sigma)\sim}(\theta)}{\sqrt{\xi_0}},$$

$$\delta A = \sum_{k,l} \left[\sum_{i,j} \widetilde{b_{ik}} \widetilde{b_{jl}} \int_{-\theta_u}^{\theta_o} f_{.i}^{(\sigma)\sim}(\theta) \bullet f_{.j}^{(u)\sim}(\theta) \, d\theta \right] v_k(\xi_0) \delta v_l(\xi_0).$$

Note that the new variables $\widetilde{C}_i$ depend on ξ_0 ($\widetilde{C}_i = \widetilde{C}_i(\xi_0)$) while C_i are constants. On the other hand it is interesting to remark the ξ_0- dependence of $\boldsymbol{u}$ and $\boldsymbol{\sigma}$ and the ξ_0- independence of $\widetilde{b_{ik}}$ which was shown by Scherzer and Meyer (1996). That means the stiffness actions do not depend on the distance from the singularity. These circumstances

remain the same even if the roots λ_i of the solvability condition are complex. To see this one has to combine the corresponding complex and conjugate complex roots and eigenvectors. For effective computations of finite element stiffness matrices additional orthogonalization of function systems $\mathbf{f}_i^{(\sigma)}(\theta)$ and $\mathbf{f}_i^{(u)}(\theta)$ leads to $\overline{\mathbf{f}_i^{(\sigma)}}(\theta)$ and $\overline{\mathbf{f}_i^{(u)}}(\theta)$ by

$$\int_{-\theta_u}^{\theta_o} \overline{\mathbf{f}_i^{(\sigma)}}(\theta) \bullet \overline{\mathbf{f}_j^{(u)}}(\theta)\, d\theta = \delta_{ij}. \tag{5}$$

As conclusion of (5) the displacements, stresses and δA result in

$$\boldsymbol{u}(\xi,\theta)_{|\xi=\xi_0} = \sqrt{\xi_0} \sum_i \overline{C_i}\,\overline{\mathbf{f}_i^{(u)}}(\theta),\ \boldsymbol{\sigma}(\xi,\theta)_{|\xi=\xi_0} = \frac{1}{\sqrt{\xi_0}} \sum_i \overline{C_j}\,\overline{\mathbf{f}_i^{(\sigma)}}(\theta), \tag{6}$$

$$\begin{aligned} \delta A &= \xi_0 \sum_i \overline{C_i}\delta\overline{C_i} \\ &= \xi_0 \sum_i \int_{-\theta_u}^{\theta_o} \left(\overline{\mathbf{f}_i^{(\sigma)}}(\theta) \bullet \frac{\mathbf{u}(\xi_0,\theta)}{\sqrt{\xi_0}}\right) d\theta \int_{-\theta_u}^{\theta_o} \left(\overline{\mathbf{f}_i^{(\sigma)}}(\theta) \bullet \frac{\delta\mathbf{u}(\xi_0,\theta)}{\sqrt{\xi_0}}\right) d\theta, \end{aligned} \tag{7}$$

$$\overline{C_i} = \int_{-\theta_u}^{\theta_o} \overline{\mathbf{f}_i^{(\sigma)}}(\theta) \bullet \frac{\mathbf{u}(\xi_0,\theta)}{\sqrt{\xi_0}} d\theta. \tag{8}$$

Relation (7) allows an excellent determination of the wanted stiffness actions in δA after a possible choise of $\theta-$ finite element approximation for $\boldsymbol{u}(\xi_0,\theta)$:

$$\mathbf{u}(\xi_0,\theta) = \sum_k \mathbf{N}_k(\theta) v_k(\xi_0)$$

with $\mathbf{N}_k(\theta)$ as one-dimensional vector shape functions at the circle $\xi = \xi_0$ which are given for instance by Zienkiewicz (1984). Then δA and $\overline{C_i}$ get the representations:

$$\begin{aligned} \delta A = \sum_{k,l} \Bigg[\sum_i & \int_{-\theta_u}^{\theta_o} \left(\overline{\mathbf{f}_i^{(\sigma)}}(\theta) \bullet \mathbf{N}_k(\theta)\right) d\theta \\ & \int_{-\theta_u}^{\theta_o} \left(\overline{\mathbf{f}_i^{(\sigma)}}(\theta) \bullet \mathbf{N}_l(\theta)\right) d\theta \Bigg] v_k(\xi_0)\delta(v_l(\xi_0)) \end{aligned} \tag{9}$$

$$\overline{C_i}(\xi_0) = \sum_k \int_{-\theta_u}^{\theta_o} \frac{1}{\sqrt{\xi_0}} \overline{\mathbf{f}_i^{(\sigma)}}(\theta) \bullet \mathbf{N}_k(\theta) d\theta\, v_k(\xi_0). \tag{10}$$

Thus the wanted stiffness actions q_{kl} can be calculated by:

$$q_{kl} = \sum_i \int_{-\theta_u}^{\theta_o} \left(\overline{\mathbf{f}_i^{(\sigma)}}(\theta) \bullet \mathbf{N}_k(\theta)\right) d\theta \int_{-\theta_u}^{\theta_o} \left(\overline{\mathbf{f}_i^{(\sigma)}}(\theta) \bullet \mathbf{N}_l(\theta)\right) d\theta. \tag{11}$$

Of course the invariant stiffness independence on ξ_0 mentioned above is still valid. This circumstance is very important in applications where invariant fracture parameters have to be introduced.
The calculation of the constants C_i from $\overline{C_i} = \overline{C_i}(\xi_0)$ is possible by the help of (8) and

$\mathbf{u}(\xi,\theta) = \sum_j C_j \mathbf{f}_j^{(u)}(\xi,\theta)$. For the roots $\lambda_1 = \alpha_1$, $\lambda_2 = \alpha_2$, $\lambda_3 = \alpha_3 + \imath\beta_3$, $(\imath = \sqrt{-1})$, $\lambda_4 = \alpha_3 - \beta_3\imath, \ldots$, $\alpha_1 < \alpha_2 < \alpha_3 \ldots$ the following system of equations is valid:

$$\begin{aligned} \overline{C_1} &= \xi_0^{\alpha_1+\frac{1}{2}} K_{11}C_1 + \xi_0^{\alpha_2+\frac{1}{2}} K_{12}C_2 + \xi_0^{\alpha_3+\frac{1}{2}}(K_{13}C_3 + K_{14}C_4) + \ldots. \\ \overline{C_2} &= \xi_0^{\alpha_2+\frac{1}{2}} K_{22}C_2 + \xi_0^{\alpha_3+\frac{1}{2}}(K_{23}C_3 + K_{24}C_4) + \ldots. \\ \overline{C_3} &= \xi_0^{\alpha_3+\frac{1}{2}}(K_{33}C_3 + K_{34}C_4) + \ldots. \\ \overline{C_4} &= \xi_0^{\alpha_3+\frac{1}{2}} K_{44}C_4 + \ldots. \\ \vdots &= \qquad\qquad\qquad\qquad\qquad\qquad\qquad\qquad\qquad\qquad \vdots \end{aligned} \tag{12}$$

In (12) the quantities $K_{ij} = K_{ij}(g_{kl})$ in general depend on the integrals g_{kl} over the scalar product of the functions $\mathbf{g}_k^{(\sigma)}(\theta)$ and $\mathbf{g}_l^{(u)}(\theta)$ which are the θ-dependent parts of the eigenfunctions $\mathbf{f}_l^{(u)}(\xi,\theta)$ and $\mathbf{f}_k^{(\sigma)}(\xi,\theta)$ by:

$$g_{kl} = \int_{-\theta_u}^{\theta_o} \mathbf{g}_k^{(\sigma)}(\theta) \bullet \mathbf{g}_l^{(u)}(\theta) d\theta.$$

The fact that $K_{21} = K_{31} = K_{32} = K_{41} = \ldots = 0$ is a consequence of the orthogonalized eigenfunction system construction. If $u(\xi_0,\theta)$ is known from the global solution of the solid $\overline{C_i}$ can be determind by (8) or (10) and C_i follow from (12).
After introducing

$$D_i = K_{ii}C_i,\ d_{ji} = \frac{K_{ji}C_i}{D_j}$$

the displacements and stresses get the representations at $\xi = \xi_0$

$$\mathbf{u}(\xi_0,\theta) = \xi_0 \sum_j D_j \xi_0^{\alpha_j}(1 + d_{jj+1}\xi_0^{(\alpha_{j+1}-\alpha_j)} + \ldots)\overline{\mathbf{f}_j^{(u)}}(\theta), \tag{13}$$

$$\boldsymbol{\sigma}(\xi_0,\theta) = \sum_j D_j \xi_0^{\alpha_j}(1 + d_{jj+1}\xi_0^{(\alpha_{j+1}-\alpha_j)} + \ldots)\overline{\mathbf{f}_j^{(\sigma)}}(\theta). \tag{14}$$

It is remarkable that in (13) and (14) the form of the concrete roots λ_i (real or conjugate complex) is not significant. These invariant ξ_0-relations can be used in fracture applications characterizing stress conditions and critical states.

EXAMPLE OF AN INTERFACE CRACK

The theoretical results described above were implemented in a computer program on heavy parallel computers. Using the Domain Decomposition (DD) as parallelizing concept the effective parallel preconditioned conjugate gradient method developed by Meyer (1990) for high order degree of freedom finite element systems is applied. In this connection the asymptotic stiffness actions determined above fit well in the parallel solution technique and lead to an improvement of the condition for the main stiffness matrices. This fact is very important for elastic-plastic statements where the linearized equations are to be solved repeatedly because the computing time can be reduced.
Results of test calculations will be explained. An interface crack specimen (750*1500 dimensionless extension, crack in the middle of the specimen with a length of 375) is strained homogenously at the elastic softer specimen end and clamped right opposite at the elastic

harder specimen end.

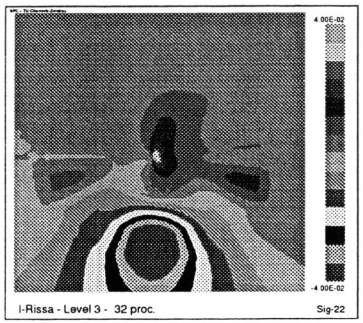

Fig. 2. $\xi_0 = 0.75$

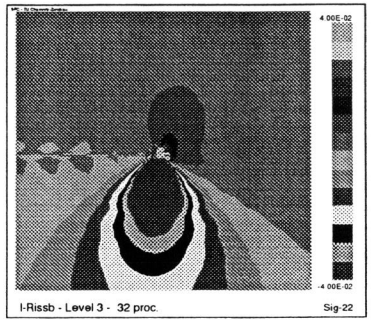

Fig. 3. $\xi_0 = 0.075$

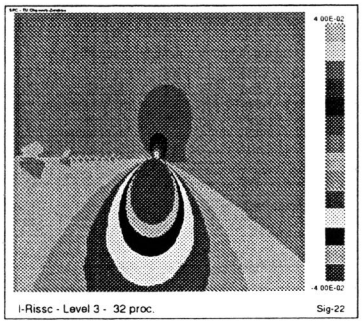

Fig. 4. $\xi_0 = 0.0075$

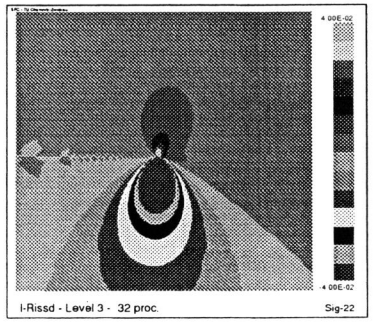

Fig. 5. $\xi_0 = 0.00075$

For pure elastic calculations the following material parameters were used:

$$\boxed{\eta = 0.0505,\ \kappa^o = 4.5,\ \kappa^u = 3.25}$$

η is the ratio of the applied shear moduli (μ), κ^o and κ^u are the ratios of bulk and shear modulus multiplied by 3/2 of the elastic softer and elastic harder specimen half. Then the roots of the solvability condition get the values:

$$\boxed{\lambda_i = -0.5 \pm i0.06591194,\ 0.0,\ 0.5 \pm i0.06591194,\ 1,\ 1.5 \pm i0.06591194,\ 2,\ \ldots}$$

The Figs. 2 to 5 show the stress fields σ_{yy} (the $y-$axis is perpendicular to crack and interface) related to μ of the elastic softer material for different ξ_0 and equal zoom radii $\xi_z = 1.0$. The crack tip lies in the centre of the Figs. and the interface on the horizontal straight line (x-axis) on the right side as prolongation of the crack. For all further Figs. the same conventions are used. The zipper like domains on both crack flanks result from postprocessing approximation errors. It should be mentioned that stresses are calculated first in Gauss points (best approximation) and then extrapolated to node points.

If in Figs. 3 to 5 one changes ξ_z from 1.0 to 0.1, 0.01 and 0.001, respectively, for a corresponding stress scale in all of these 3 cases the same Fig. 2 will be produced illustrating the stiffness independence on ξ_0 shown above. On the other hand the Figs. 2 to 5 express convergent stress fields at interface crack tip.

Further the pressure stresses ($\sigma_{yy} < 0$) under the crack tip are remarkable. They result from the different Poisson effect in both material domains. Both the soft material and the hard one are exposed to tension in $y-$direction which causes different contractions in $x-$direction. At the interface crack tip the hard material impedes the contractions of the soft one and gets the pressure stresses as a reaction to this impediment. For comparison Fig. 6 shows the $\sigma_{yy}-$field from the solution without considering the special eigenfunction solution representations ($\xi_z = 1.0$). It can be seen that pressure stresses appear in a small region under the crack flank only.

To bear out that usual finite element methods without special asymptotics cannot give correct solutions at interface cracks geometrically the same interface crack specimen with almost identical material behaviour of the soft and hard regions is considered. The material parameters are chosen as

$$\boxed{\eta = 0.7194,\ \kappa^o = 4.5,\ \kappa^u = 3.25}$$

which get the roots λ_i:

$$\boxed{\lambda_i = -0.5 \pm i0.001687346,\ 0.0,\ 0.5 \pm i0.001687346,\ 1,\ 1.5 \pm i0.001687346,\ 2,\ \ldots}$$

The load is defined as symmetrical $y-$displacement at the specimen boundaries. The comparable $\sigma_{yy}-$stress fields with and without asymptotics are given in Figs. 7 and 8 ($\xi_z = 1.0$, $\xi_0 = 0.75$). The pure finite element calculations represent the known solution of a mode-I "homogenous" crack. The Poisson effect consequences do not appear. In the Fig. 8 "with asymptotics" they can be seen in the region $\xi < 0.4$. In Fig. 9 the $\sigma_{yy}-$stresses "with asymptotics" of the same specimen are shown but the Poisson effect consequences are deleted by special displacement defintion at the lower right edge of the specimen boundary in the hard material region. The defintion of these displacements is demonstrated by arrows in Fig. 10. They cause negative $x-$displacements directly above the interface and crack tip, push back the $x-$contractions in the soft material region and are able to balance the $x-$ displacements below and above the interface crack tip this way. Thus the Poisson effect consequences vanish and Fig. 9 shows the solution of a mode-I "homogenous" crack.

We have seen that the asymptotic solution technique presented here is able to give correct stress fields for interface cracks under tension with and without Poisson effect consequences by the help of the same eigenfunctions. The pure finite element approach is too coarse to feel the described effects. Also mesh refinement cannot save the situation of usual finite elements at interface cracks because they produce wrong asymptotic behaviour at the tip. In connection with the chosen material parameters this behaviour affects the surrounding body more or less.

This fact can also be deduced from the comparison of the stress fields σ_{xx} and σ_{xy} with and without special asymptotics in the solution technique. The corresponding results are shown in Figs. 11 to 14 ($\xi_0 = 0.0075$, $\xi_z = 1.0$). The material parameters are chosen from

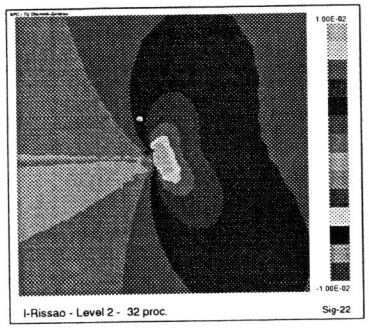

Fig. 6. σ_{yy} for the interface crack without asymptotics

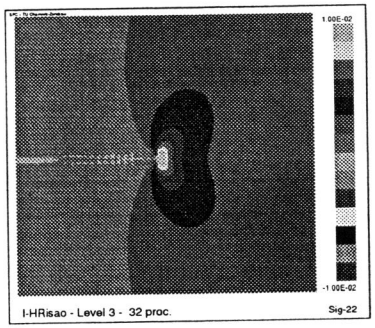

Fig. 7. σ_{yy} for the almost "homogenous" crack without asymptotics

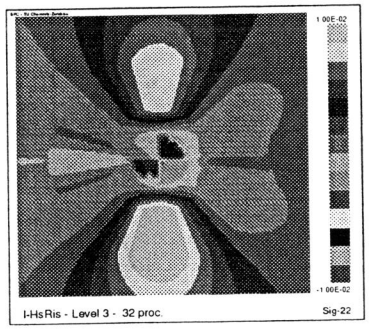

Fig. 8. σ_{yy} for the almost "homogenous" crack with asymptotics

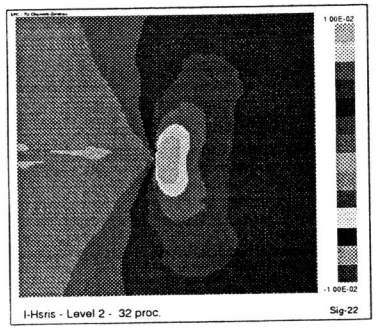

Fig. 9. σ_{yy} for the almost "homogenous" crack with asymptotics after deleting Poisson effect consequences

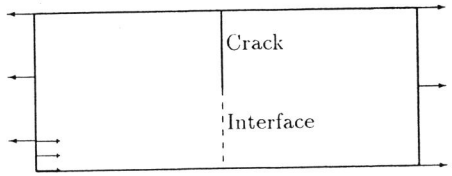

Fig. 10. "Kinematical" remove of the Poisson effect consequences

the first "real" interface crack specimen. It is interesting to note the position of the $y-$axis in these stress fields below the $x-$axis of Fig. 11 and Fig. 13. For σ_{xy} the $y-$axis is a zero line. On the other hand σ_{xx} has 2 symmetrical zero lines starting from the crack tip. These effects of symmetry (σ_{xx}) and antisymmetry (σ_{xy}) do not appear in the pure finite element calculations which can bee seen in Fig. 12 and Fig. 14.
It is clear that the circumstances described above have corresponding consequences for the deformation field around the interfacecrack tip allowing non-linear constitutive behaviour on the basis of flow theory. Let us consider the specimen above in the plastic deformation

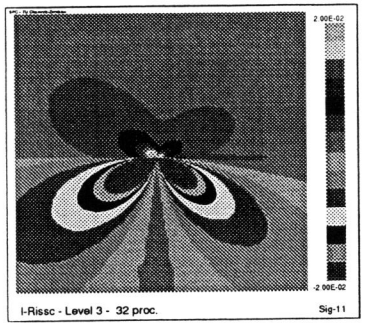

Fig. 11. σ_{xx} with asymptotics

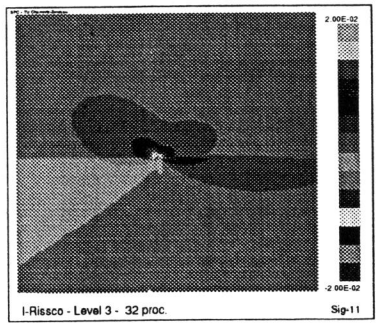

Fig. 12. σ_{xx} without asymptotics

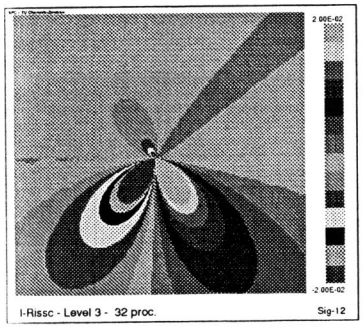

Fig. 13. σ_{xy} with asymptotics

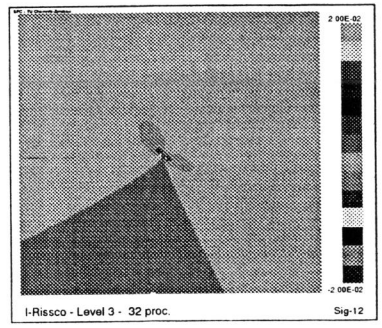

Fig. 14. σ_{xy} without asymptotics

range. The elastic material parameters coincide with those of the "real" interface crack specimen. The plastic hardening is characterized by the yield function f in the form

$$f(\tilde{\tau},\chi) = \left\{ \begin{array}{lcl} \tilde{\tau} - \tau_t^u - b^u \chi^{\rho^u} & : & \theta < 0 \\ \tilde{\tau} - \tau_t^o - b^o \chi^{\rho^o} & : & \theta > 0 \end{array} \right\} = 0$$

with $\chi = \int \sqrt{\frac{4}{3} \sum_{i,j} d\epsilon_{ij}^{(pl)} d\epsilon_{ij}^{(pl)}}$ as the Odkvist parameter. $\epsilon_{ij}^{(pl)}$, $\tilde{\tau}$, τ_t^u and τ_t^o denote plastic strain tensor components, the octahedron stress τ ($\tau = \sqrt{\frac{1}{3} S_{ij} S_{ij}}$, $S_{ij}-$ components of the stress deviator) related to μ of the elastic softer material and corresponding yield stresses, respectively. For the material parameters:

$$\boxed{\tau_t^u = \tau_t^o = 0.245,\ b^u = 1.798,\ b^o = 0.01666,\ \rho^u = 0.25,\ \rho^o = 0.4}$$

the following roots λ_i can be deduced:

$$\boxed{\eta = 0.01,\ \kappa^o = 225,\ \kappa^u = 32.5}$$

$$\boxed{\lambda_i = -0.5 \pm i0.00193809,\ 0.0,\ 0.5 \pm i0.00193809,\ 1,\ 1.5 \pm i0.00193809,\ 2,\ \ldots}$$

In Fig. 15 and Fig. 16 the plastic zones at the interface crack tip of the specimen described above are presented with and without asymptotics for comparable load levels ($\xi_0 = 0.075$, $\xi_z = 0.1$).

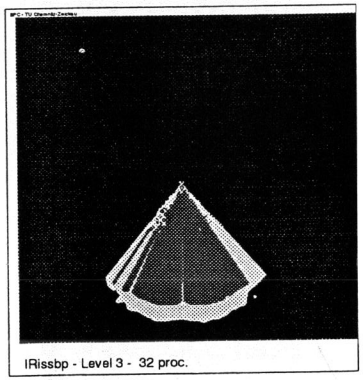

Fig. 15. Plastic zone with asymptotics

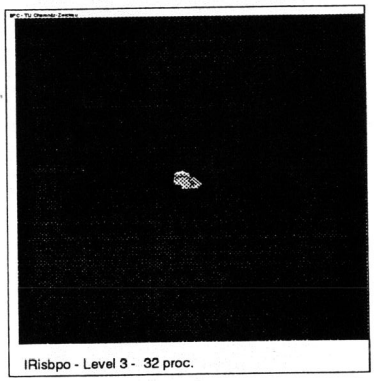

Fig. 16. Plastic zone without asymptotics

It can be seen that plastic deformations occur dominantly in the elastic harder material because the stress level is higher there. This fact cannot be found in the solution without asymptotics.

CHARACTERIZATION OF DEFORMATION AND STRESS STATES

As it is known the application of solid mechanics in modern microelectronic components leads to the task of calculation of very complicated stress and deformation fields depending on geometry, material laws, boundary conditions, loads and so on. On the other hand it must be pointed out that the calculation of stresses, strains, displacements etc. only does not give the answer to the main question:

Does the structure fail or not?

To estimate fracture three points are necessary:

1. Getting exact solutions for the mathematically formulated boundary value problems.
2. These solutions must be comparable to other solutions of corresponding statements representing modified boundary conditions, material behaviour, load trajectories etc.
3. Experimental research for identification of material behaviour and determination of the critical parameters of the solid models.

The second point results from the fact that fracture occurs in strong connection to local stress and deformation states. In other words it is necessary to characterize the possible local stress and deformation states for different fracture situations. When applying non-linear deformation models this fact is very important. For example using the flow theory where material behaviour depends on local load trajectories the stress conditions change during the loading process and can result in different possible local stress states of fracture. To describe these circumstances let us introduce main stresses. The main stresses σ_1, σ_2

and σ_3 related to von Mieses stress ($\sigma_v = \frac{3}{\sqrt{2}}\tau$) can be expressed by the constraint factor ($h = \frac{\sqrt{2}(\sigma_{xx}+\sigma_{yy}+\sigma_{zz})}{6\tau}$, σ_{xx}, σ_{yy} and σ_{zz} are the normal stress components in a $xyz-$co-ordinate system) and the similarity angle of stress deviator ($\omega = \frac{1}{3}\arccos\frac{\sqrt{2}S_{ij}S_{ik}S_{kj}}{3\tau^3}$):

$$\begin{aligned}\sigma_1 &= h + \tfrac{2}{3}\cos(\omega)\\ \sigma_2 &= h + \tfrac{2}{3}\cos(\omega - \tfrac{2\pi}{3})\\ \sigma_3 &= h + \tfrac{2}{3}\cos(\omega - \tfrac{4\pi}{3}).\end{aligned} \tag{15}$$

Note that these representations are independent of concrete material laws. Main stresses are the roots of the corresponding eigenvalue equation of stress tensor. For two-dimensional plane strain conditions the constraint factor and the similarity angle are interdependent. Thus it can be shown that in this case the deformation components e_{xx}, e_{yy} and e_{xy} ($e_{zz} = 0$) for isotropic deformation theory materials have the the following representations:

$$\begin{aligned}e_{xx} &= \tfrac{6\gamma(\tau)}{8}[\sin(2\alpha - \omega + \tfrac{\pi}{3}) + \cos(2\alpha + \omega + \tfrac{\pi}{3}) + 2\sqrt{3}\sin(\omega + \tfrac{\pi}{6})]\\ e_{yy} &= \tfrac{6\gamma(\tau)}{8}[\sin(2\alpha - \omega + \tfrac{\pi}{3}) + \cos(2\alpha + \omega + \tfrac{\pi}{3}) - 2\sqrt{3}\sin(\omega + \tfrac{\pi}{6})]\\ e_{xy} &= \tfrac{6\gamma(\tau)}{8}[\cos(2\alpha - \omega + \tfrac{\pi}{3}) - \sin(2\alpha + \omega + \tfrac{\pi}{6})].\end{aligned} \tag{16}$$

For the flow theory (16) is analogical using the corresponding increments. The angle α which depends on stress components ($\tan(2\alpha) = \frac{2\sigma_{xy}}{\sigma_{xx}-\sigma_{yy}}$) characterizes the location of main stress axes referring to the arbitrary $xy-$ co-ordinate system and γ as a function of τ represents the octahedron shear ($\gamma = \sqrt{\frac{4}{3}\epsilon_{ij}\epsilon_{ij}}$, $\epsilon_{ij}-$ components of the deformation deviator). From these relations it can be seen that the deformation components which qualify the solid straining can be calculated if τ, κ and α are known. τ acts as an amplitude characterizing the magnitude of strains and κ and α which are finite in singular points specify the kind of deformation. If one puts the asymptotic expansions above into τ it can be concluded that the magnitude of deformation is only dominated by coefficients of the first eigenfunctions because of the discrete solvability condition roots λ_i. These facts suggest the following fracture analysis for solids:

1. Determination of $\mathbf{u}(\xi, \theta)$ from the whole solution of the body by finite elements or other methods taking into consideration the correct asymptotic behaviour using the stiffness actions described above which do not depend on the distance to the considered point.
2. Computation of $\overline{C_i}$ by (8) or (10).
3. Calculation of C_i by the triangle system (12) $\overline{C_i} = K_{ij}C_j$ with $K_{ij} = K_{ij}(g_{ij})$.
   - g_{ij} can be interpreted as "inner deformation metric" of the local point.
   - $C_i \approx \frac{\overline{C_i}}{K_{ii}}\xi_0^{-(\alpha_i+\frac{1}{2})}$ is valid for small ξ_0.
4. C_i are the fracture parameters which get critical values in failure situations. Because of (8), (12) and g_{ij} they express integral magnitudes of the stress and deformation field around the considered point. C_1 acts as the main factor (and if the root λ_1 is double then C_1 and C_2 both do) and the other ones operate as higher order moments.
5. κ and α characterize critical stress states for the critical C_i-values. If such critical C_i-values are determined in an experimental way together with the numerical technique mentioned above then fracture predictions are only possible in connection with the realized κ and α.

On Fig. 17 and Fig. 18 the distribution of the two parameters ($\tan(\alpha)$, $\cos(3\omega)$) characterizing stress and deformation states of the pure elastic specimen solution at interface crack tip presented above are given. It can be shown that these Figs. remain the same for arbitrary load values of the specimen in the linear material law case provided the "form" of boundary conditions does not change.

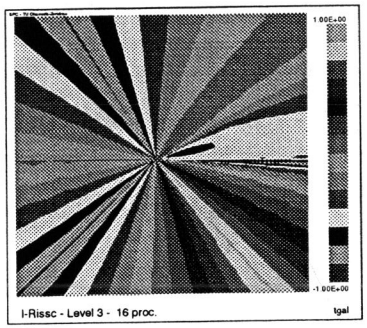

Fig. 17. $\tan(\alpha)$ at interface crack tip

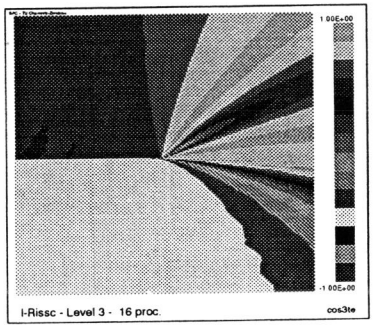

Fig. 18. $\cos(3\omega)$ at interface crack tip

If non-linear material behaviour (flow theory) was applied they would change during loading for the same "form" of boundary conditions characterizing different stress conditions (local load trajectory). This way they distinguish critical fracture states if the realized boundary value problem for any load level corresponds to failure at the interface crack tip.

Summarizing it can be concluded that macroscopic fracture estimation of solids leads to the question of describing deformations by solid models at critical points. If this question is solved, that means the constitutive behaviour is known, the corresponding fracture characteristics result from the asymptotic analysis presented above.
Extensions of the concepts described in this paper to geometrically non-linear material behaviour, anisotropic material laws and three-dimensional boundary value problems are possible as it was mentioned by Scherzer and Meyer (1996). However their realization can only be done in the future.

REFERENCES

Scherzer, M. (1994). Asymptotic equations for the isotropic hardening flow theory in singular points. *ZAMM*, **74**, pp. T184–T186.

Scherzer, M. and Meyer, A. (1996). Zur Berechnung von Spannungs- und Deformationsfeldern an Interface-Ecken im nichtlinearen Deformationsbereich auf Parallelrechnern. *TU Chemnitz-Zwickau, Preprint-Reihe des Sonderforschungsbereiches 393 „Numerische Simulation auf massiv parallelen Rechnern"*, SFB393/96-03, Chemnitz.

Korn, G.A. and Korn, T.M. (1968). *Mathematical Handbook.* McGraw-Hill Book Company, London.

Zienkiewicz, O.C. (1984). *Methode der finiten Elemente*, VEB Fachbuchverlag, Leipzig.

Meyer, A (1990). A parallel preconditioned conjugate gradient method using domain decomposition and inexact solvers on each subdomain. *Computing*, **45**, pp. 217–234.